J Mater Sci (2006) 41:6591–6598
DOI 10.1007/s10853-006-0198-1

Meso-macro approach for composites forming simulation

Philippe Boisse

Published online: 28 September 2006

Abstract The F.E. analysis of woven composite reinforcement forming is an alternative to geometrical draping computation. It permits to account for mechanical behaviours of the fabric and static boundary conditions of the process. In this paper, macroscopic forming simulations of woven composite reinforcements are performed using finite elements composed of woven cells, the mechanical behaviour of which are computed by F.E. analyses at mesoscale i.e. on the unit cell of the fabric. The objective is to only calculate the relevant quantities in the woven finite element. The in-plane biaxiale tensile behaviour and the in-plane shear behaviour are obtained by 3D analyses of the woven cell submitted respectively to tension and shear. They need to take the specificities of the mechanical behaviour of the yarn (made of thousand of fibres) into account. Especially an objective derivative based on the fibre rotation is used. These computations on the unit woven cell have proved to be consistent with experimental tests. An example of deep drawing of a square box using the proposed approach is presented. Angles between warp and weft directions are computed as well as wrinkles.

Introduction

Textile reinforcements of composites are especially efficient in case of double curve geometries because of the interlacing of warp and weft yarns. Because it is made of woven yarns, the fabric can reach very large in-plane shear strain. The fabric is also submitted to tensions but, due to the large tensile stiffness, the associated axial strains are usually small especially in the cases of classic composite reinforcements made of glass, aramid or carbon. In the objective of the development of composite forming simulation codes, an important effort is currently made to model and simulate the large deformations of textile reinforcements. Actually this fabric forming is essential in textile composite manufacturing. During the forming stage the possible deformation modes of the composite are those of the reinforcement because of the absence of cohesion of the matrix. This one is not polymerised (in case of prepregs), heated over the melting point (in case of thermoplastics) or absent (in case of the first stage of LCM processes). A composite forming simulation code has to determine the conditions of the feasibility of a process without defect but also to know the positions of the reinforcements after shaping. These positions (directions and densities) strongly condition the permeability of the reinforcement and thus the filling of the resin in the case of a liquid moulding process [1, 2]. In addition, the angles between warp and weft yarns and the fibre densities have a large influence on the mechanical behaviour of the final textile composite structure.

The codes that are the most commonly used in industry for fabric forming simulations, are based on geometrical approaches (fishnet algorithms) [1, 3–5]. In these methods, the knowledge of the shape on which the fabric is formed and initial geometrical conditions leads to the positions of the yarns on the final form. The length of the yarns is constant and the rotation of warp and weft yarn at each intersection is free. This leads to a local geodesic problem that is generally non-linear but very small and the resolution is very fast. The computed shear angle can be

P. Boisse (✉)
Laboratoire de Mécanique des Contacts et des Solides,
INSA de Lyon, 27 avenue Jean Capelle, 69621 Villeurbanne Cedex, France
e-mail: Philippe.Boisse@insa-lyon.fr

compared to the locking angle of the fabric. These approaches are fairly efficient especially in the case of hand operated draping of classic fabrics or prepregs. Nevertheless they do not account neither for the mechanical behaviour of the fabric nor for the loads on the boundary that can be very important to achieve a correct draping [6].

In order to avoid these drawbacks, the fabric forming can be simulates within a finite element approach [7–9]. This requires the knowledge and modelling of the mechanical behaviour of woven reinforcements. These are highly specific because of the internal structure of the fabrics. It is a multi-scale problem. The macroscopic behaviour is much dependent of the interactions of yarns at meso-scale (scale of the woven unit cell) and at the micro-scale (level of the fibres constituting yarns). Despite a lot of works in the field, there is no widely accepted model that describes accurately all the main aspects of fabric mechanical behaviour [10]. A lot of the models are based on the woven and multi-scale nature of the textile. Some approaches are based on a discrete modelling of the fabric. The yarns (or the fibres [11]) are assumed to be straight or curved beams or truss connected by tensional and rotational springs. If these approaches have been widely used to analyse the mechanical behaviour of the unit woven cell [12–15], in the objective of forming simulations, they have also been extended to the discrete modelling of the whole textile structure that is represented by a network of interwoven trusses or beams with different springs [16, 17]. The global textile structure deformation can be computed if the models used for local components are simple enough. This is the limit of this approach that can account with difficulty for the complexity of the woven cell behaviour. The composition of the yarn made of many fibres and to the weaving cannot be accurately described by straight trusses and springs. An opposite alternative consists in considering the fabric as an anisotropic continuum, the model of which is obtained by homogenizing the mechanical behaviour of the underlying meso-structure [8, 10, 18, 19]. These continuum models can be implemented in classic shell or membrane finite elements. Nevertheless the identification of the homogenized material parameters is not easy. The main difficulty is due to the variation of the mechanical behaviour when the fabric is strained and when, consequently, the directions and the density of the yarns change.

In this paper, a mesoscopic analysis of the woven unit cell is associated to a finite element assumption. Specific elements are made of woven unit cells. Mesoscopic analyses of the mechanical behaviour of these woven cells are performed by 3D F.E. computations of the woven cell possibly associated with experiments. This local behaviour and the corresponding strain energy in the strain field of the finite element gives the nodal interior loads. Only tensile and in plane shear deformation energy are taken into account. The bending energy of the woven reinforcement is neglected because the yarns made of thousand of fibres the diameter of which is very small (5–7 μm for carbon and 5–25 μm for glass).

The mesoscopic F.E. analyses of the woven unit cell are presented. They are not standard computations because of the composition of the yarn that is not a classic continuous media. The results are compared to experiments. Then from these analyses, the finite elements made of woven cells are used for forming simulations.

Finite element made of woven cells

The element presented Fig. 1 is made of ncell^e woven cells. It is a four node element with classic bilinear interpolation functions:

$$N^1 = \frac{1}{4}(1-\xi_2)(1-\xi_1) \quad N^2 = \frac{1}{4}(1-\xi_2)(1+\xi_1)$$
$$N^3 = \frac{1}{4}(1+\xi_2)(1+\xi_1) \quad N^4 = \frac{1}{4}(1+\xi_2)(1-\xi_1) \quad (2.1)$$

A three node element has also been developed based on the same approach and linear interpolation function [6]. The natural coordinates of the element ξ_1, ξ_2 and consequently the edges of the element follow the directions of the yarns. It has also been shown that otherwise a locking can appear due to the stiffness in the two yarn directions that is very much larger than others [20]. Secondly, this will lead to a better numerical efficiency.

The element is made of unit woven cells. The mechanical behaviour of those woven cells will be analysed at mesoscale in Section ''Finite element analyses at the mesoscopic level''. Because the fabric reinforcement is made of woven yarns that are themselves made up of thousand of fibres, there are possible relative displacements and only the tensile strain energy and the in-plane shear strain energy are taken into account in the finite element. The virtual work of interior loads for a woven cell in a virtual displacement η can be written:

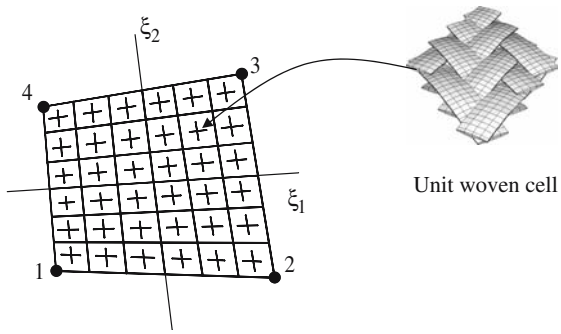

Fig. 1 Bilinear finite element made of woven cells

$$W_{\text{int}}^{\text{cell}}(\eta) = \varepsilon_{11}(\eta) T^{11} L_1 + \varepsilon_{22}(\eta) T^{22} L_2 + \gamma(\eta)\, C \qquad (2.2)$$

T^{11} and $T^{22}$are the tension in warp and weft directions, $\varepsilon_{11}(\eta)$ and $\varepsilon_{22}(\eta)$ are the axial strains in the warp and weft directions in the virtual displacement field η. γ (η) is the virtual rotation angle between warp and weft directions and C is the couple due to in plane shear in the unit cell. The finite element approach presented in the present work is based on an explicit scheme, consequently the nodal elementary interior loads $F_{\text{int}}^{\text{e}}$ are the only needed quantities. They are given by the interior elementary virtual work $W_{\text{int}}^{\text{e}}$ which is the sum of the virtual work on each unit cell :

$$\begin{aligned} W_{\text{int}}^{\text{e}}(\eta) = & \sum_{p=1}^{\text{ncell}^{\text{e}}} {}^{p}\varepsilon_{11}(\eta)\, {}^{p}T^{11}\, {}^{p}L_1 + {}^{p}\varepsilon_{22}(\eta)\, {}^{p}T^{22}\, {}^{p}L_2 \\ & + \sum_{p=1}^{\text{ncell}^{\text{e}}} {}^{p}\gamma(\eta)\, {}^{p}C = \eta_s (F_{\text{int}}^{\text{e}})_s \end{aligned} \qquad (2.3)$$

The nodal index s varies from 1 to 12 in the case of the four node quadrilateral.

Denoting g_α the covariant material vectors such as $g_\alpha = \frac{\partial x}{\partial \xi_\alpha}$ and g^α the related contravariant vectors (α and β indexes take values 1 and 2), the strain interpolation components $B_{\alpha\beta s}$ define the virtual strain components $\bar{\varepsilon}_{\alpha\beta}$ from the virtual displacement components:

$$\bar{\varepsilon}_{\alpha\alpha}(\eta) = B_{\alpha\alpha s}\eta_s \quad \text{and} \quad \gamma(\eta) = B_{\gamma s}\eta_s \qquad (2.4)$$

with

$$\begin{aligned} B_{\alpha\alpha s} = \frac{\partial N^k}{\partial \xi_\alpha}(g_\alpha)_m \quad & k = \text{integer part of}\left(\frac{s+2}{3}\right) \\ & \text{and } m = s - 3(k-1) \end{aligned} \qquad (2.5)$$

$$\begin{aligned} B_{\gamma s} = & \frac{\partial N^k}{\partial \xi_1}\left[\cot g\theta \frac{(g_1)_m}{\|g_1\|^2} - \frac{(g_2)_m}{\sin\theta \|g_1\| \|g_2\|}\right] \\ & + \frac{\partial N^k}{\partial \xi_2}\left[\cot g\theta \frac{(g_2)_m}{\|g_2\|^2} - \frac{(g_1)_m}{\sin\theta \|g_1\| \|g_2\|}\right] \end{aligned} \qquad (2.6)$$

The nodal interior loads are related to tension in the yarns and shear couple by:

$$\begin{aligned} \left(F_{\text{int}}^{\text{e}}\right)_s = & \sum_{p=1}^{n_t} \frac{1}{\|g_1\|} {}^{p}B_{11s}\, {}^{p}T^{11} + \sum_{p=1}^{n_c} \frac{1}{\|g_2\|} {}^{p}B_{22s}\, {}^{p}T^{22} \\ & + \sum_{p=1}^{n_t n_c} {}^{p}C\, {}^{p}B_{\gamma s} \end{aligned} \qquad (2.7)$$

Accounting for the bilinear interpolation, the summation can be done on only four crossovers, the positions of which depend on the warp and weft number of yarns (n_c and n_t). Details of the calculations can be found in [21]. The nodal interior load components are given explicitly without any matrix multiplication, and without computing terms equal to zero (due to zero stiffness). This is important with regard to the numerical efficiency.

To make a finite element simulation of composite woven reinforcement forming (macroscopic analyses) based on the above approach, it is necessary to be able to calculate the tensions T^{11} and T^{22} and the shear couple C for a given strain field in the woven unit cell. It is assumed that the tension do not depend on the shear angle and that the shear couple do not depend on the axial strain i.e. $T^{11}(\varepsilon_{11}, \varepsilon_{22})$, $T^{22}(\varepsilon_{11}, \varepsilon_{22})$ and C (γ). In [22], biaxial tensile tests performed for different angle between warp and weft yarns have shown that the influence of this angle is small and can be neglected. The second assumption (C only depending on γ) is probably less true [23, 24]. Nevetheless, all the experimental results that are currently available give the shear load in function of the shear angle without any information on the tensions, so the assumption $C(\gamma)$ will be made by default. The next section will have the objective to determine the biaxial tensile behaviour $T^{11}(\varepsilon_{11}, \varepsilon_{22})$, $T^{22}(\varepsilon_{11}, \varepsilon_{22})$ and the in plane shear behaviour C(γ) by 3D F.E. analyses performed at the mesoscopic level i.e. on the unit woven cell.

Finite element analyses at the mesoscopic level

Characteristics of the analysis

Virtual tests are performed at the mesoscopic level. 3D finite elements analyses are made on a unit woven cell (representing the periodicity of the fabric) under loading [25, 26]. These computations give local results within the material that are very difficult to obtain experimentally. They also allow to test materials at the design stage i.e. before their manufacture. Finally, they permit the simulation of many tests that would be costly and difficult to perform experimentally.

The analyses are not standard mainly because the yarn is not a classic continuous material but is made of thousand of fibres that can slide relatively. Nevertheless, although some works have been proposed in this direction [11], it is difficult, and in practice impossible, to model each fibre for a usual woven composite reinforcement (6000 fibres in the case of a classic 2×2 twill of carbon). Consequently a continuous approach must be used to model the yarns that are meshed with 3D elements. This equivalent mechanical

behaviour is very specific. The principal specificities of the mesoscopic F.E. analysis are listed below:

(a) most stiffnesses (bending, shear) are very small in comparison to tension stiffness in the fibres direction,
(b) the almost zero value of some stiffnesses (associated to very small strain energies) leads to numerical instabilities (zero energy modes) which must be eliminated,
(c) the important differences between longitudinal and transversal behaviours require to follow strictly the fibre directions in order to give the mechanical properties in a frame directed at each time by the current fibre directions,
(d) the longitudinal yarn tensile behaviour must be known,
(e) the yarn crushing (transverse behaviour of the yarn) must be modelled efficiently,
(f) there are some geometrical non-linearities (undulation changes, large angle variations between warp and weft directions): the analysis must be performed at finite strain,
(g) the contacts between yarns are modelled using a master/slave technique with Coulomb friction
(h) the analysis is made for a minimal elementary pattern. The boundary conditions must represent the fabric periodicity and the possible pattern symmetries.

The very small stiffnesses in bending and shear (a) can be modelled by an elastic orthotropic material, with small transverse Young's modulus (perpendicular to the fibre direction) and very small shear modulus with respect to the longitudinal Young's modulus (fibre direction). The longitudinal Young's modulus is identified using a tension test on a single yarn. The transverse Young's modulus (e) is not constant. It is the result of the transverse compaction of the fibre bundle. It is small in the initial state, but increases as a function of transverse and longitudinal strains. Therefore, the following crushing has been choosen:

$$E_\tau = E_0 \varepsilon_{11}^q |\varepsilon_{\tau\tau}|^r + E_\varepsilon \tag{3.1}$$

where τ is equal to 2 or 3, 1 is the fibre direction, 2 and 3 the transverse directions. E_ε is the initial transverse modulus (usually very small). E_0, q and r are three material parameters. Because of the difficulty to perform a compression test that is independent of the boundary conditions, these constants have been identified by an equi-biaxial tension test (see Fig. 4) coupled with an inverse method [25, 27]. Many other compaction models have been proposed, but they usually do not take the longitudinal strain into account [28, 29].

Very weak stiffnesses (close to zero) lead to zero energy modes (b). These spurious modes are classic in case finite elements using reduced integration of [30]. Some displacements fields (these spurious modes) are possible without any strain energy because they do not change the strain value at gauss points used in case of reduced integration. In the present fabric 3D finite element analyses, the zero energy modes are possible, not because of reduced integration but because some material rigidities are close to zero. The result is the same: some displacements modes correspond to zero strain energy and the computation is unstable. To avoid these spurious modes, the finite elements with reduced integration use hourglass control [31, 32]: a stabilization matrix is added to the element stiffness, based on some orthogonality properties of the added fields, to remove the spurious modes without perturbing the computation result. These approaches have proved to be efficient in the case of the present analysis.

Since displacements and strains are large, it is necessary to work within a large strain theory (f). Because Young's moduli are very different in longitudinal and transverse directions, it is important that the orthotropic axes correspond to material directions during the analyses and especially that the longitudinal direction where the rigidity is high, strictly follows the fibres (c). In that goal, as it is presented in next section, the yarn behaviour law is associated with an objective derivative based on the rotation of the fibre. This enables the fibre direction to be strictly followed, unlike approaches usually developed in the finite element codes that are based on average rotations of the matter.

Hypoelastic model for fibrous materials

As it is usual in commercial finite element codes [33] the material mechanic behaviour is an hypoelastic continuous orthotropic model at large strain. The specificity here lies in the use of the fibre rotation tensor Δ. It is used to define a strain measure of the fibrous medium and to define the evolution of the strong anisotropic direction that strictly follows the fibre direction contrary to Jaumann corotational formulation [34, 35] or Green Naghdi approach [35, 36] that are usualy used in finite element codes [33]. The rotations used in these cases (the polar rotation $\mathbf{R}$ for Green Naghdi et the rotation of the corotational frame $\mathbf{Q}$ for Jaumann) are average rotations of the matter in a given point. They are not equal to the rotation of the fibre at this point i.e. the rotation in a specific material direction. From the initial orientation of the orthotropic axes κ_i^0 (i = 1, 2 or 3), the fiber rotation Δ is used to compute the current constitutive axes κ_i^t:

$$\kappa_i^t = \Delta \cdot \boldsymbol{\kappa_i^0}. \tag{3.2}$$

Equation (3.2) leads to the set of formula (3.3) that explicitly give the constitutive axes $\{\kappa^t\}$ as functions of the initial constitutive axes $\{\kappa^0\}$ and the deformation gradient $\mathbf{F}$ ([37]):

$$\begin{cases} \kappa_1^t = \frac{\mathbf{F}\cdot e_1^0}{\|\mathbf{F}\cdot e_1^0\|} \\ \kappa_2^t = e_2^0 - \frac{b_2}{1+b_1}\left(e_1^0 + \kappa_1^t\right) \\ \kappa_3^t = e_3^0 - \frac{b_3}{1+b_1}\left(e_1^0 + \kappa_1^t\right) \\ \text{with } b_k = \kappa_1^t \cdot e_k^0 \text{ and } b_k \neq 1 \end{cases} \tag{3.3}$$

The strong anisotropic direction remains aligned with the fibre direction. The current constitutive tensor $\boldsymbol{C}$ is obtained from the initial constitutive tensor ${}^0\boldsymbol{C}$:

$$\boldsymbol{C} = \boldsymbol{R} : {}^0\boldsymbol{C} : \boldsymbol{R}^T \quad \text{with} \quad {}^0\boldsymbol{C} = {}^0C_{ijkl}\kappa_i^0 \otimes \kappa_j^0 \otimes \kappa_k^0 \otimes \kappa_l^0 \tag{3.4}$$

$\boldsymbol{R}$ is the fourth order rotation tensor computed from second order rotation tensor Δ:

$$R_{ijkl} = \Delta_{ik}\Delta_{jl}. \tag{3.5}$$

Consequently, $\boldsymbol{C}$ is known:

$$\boldsymbol{C} = {}^0C_{ijkl}\kappa_i^t \otimes \kappa_j^t \otimes \kappa_k^t \otimes \kappa_l^t \tag{3.6}$$

and the hypoelastic constitutive law is:

$$\boldsymbol{\sigma}^{\nabla} = \boldsymbol{C} : \mathbf{D} \quad \text{with} \quad \boldsymbol{\sigma}^{\nabla} = \Delta \cdot \frac{\mathrm{d}}{\mathrm{d}t}\left(\Delta^T \cdot \boldsymbol{\sigma} \cdot \Delta\right) \cdot \Delta^T \tag{3.7}$$

$\mathbf{D}$ is the strain rate tensor and $\boldsymbol{\sigma}^{\nabla}$ is the objective derivative of the Cauchy stress tensor with respect to the rotation Δ. The cumulated tensorial strain tensor $\boldsymbol{\varepsilon}$ and the cauchy stress tensor $\boldsymbol{\sigma}$ are such as:

$$\begin{aligned} \boldsymbol{\varepsilon} &= \Delta \cdot \left(\int_0^t \Delta^T \cdot \mathbf{D} \cdot \Delta \mathrm{d}t\right) \cdot \Delta^T \\ \boldsymbol{\sigma} &= \Delta \cdot \left(\int_0^t \Delta^T \cdot (\boldsymbol{C} : \mathbf{D}) \cdot \Delta \mathrm{d}t\right) \cdot \Delta^T \end{aligned} \tag{3.8}$$

It can be shown that Eq. (8) will always give a logarithmic strain in the strong anisotropic direction and ensures the summation of the stress increments along this direction. The use of the fibre rotation tensor Δ for the objective rotational derivative and the evolution laws as defined above give a consistent approach for fibrous media with one strong anisotropic direction as it is the case for the yarns of the composite reinforcements that consist in a fibre bundle. The presented approach has been implemented in the ABAQUS code using the VUMAT routine [38]. In the cases of analyses of the woven cells composed of woven yarns, it has proved to be much more efficient than the use of classic Green Naghdi or Jaumann approaches that lead to too weak results because the fibre direction is not exactly followed.

Mesoscopic F.E. analysis of a woven unit cell under biaxial tension

Figure 2b shows the mesh (30000 d.o.f.) used for the F.E. analyses of the elementary pattern of the 2×2 carbon twill (Fig. 2a). The young modulus in the fiber direction is E_0=1.1×10^5 MPa and the crushing law parameters are $m = 1$, $n = 2$. The set of analyses performed for different warp-weft ratio give the tensile surface $T^{11}(\varepsilon_{11}, \varepsilon_{22})$, or $T^{22}(\varepsilon_{11}, \varepsilon_{22})$ (Fig. 3). The two surfaces are identical because the fabric is (nearly) balanced. The tensile surface show that the tensile curves $T^{11}(\varepsilon_{11})(\varepsilon_{22}$ fixed) are clearly non-linear at the beginning of the loading. These computed tensile curves are compared to experiments for differents warp strain/weft strain ratios denoted k. The experimental biaxial tensile tests have been performed on cross shape specimen (Fig. 4) [22]. The results are in correct agreement. The crushing strain is important (45%) and is a main

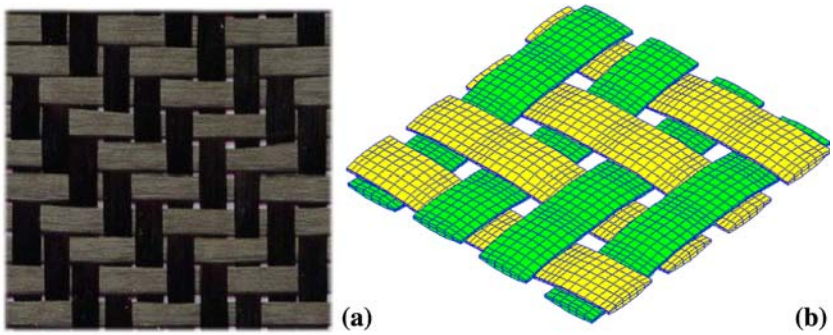

Fig. 2 (**a**) 2×2 carbon twill. (**b**) Mesh of the unit cell

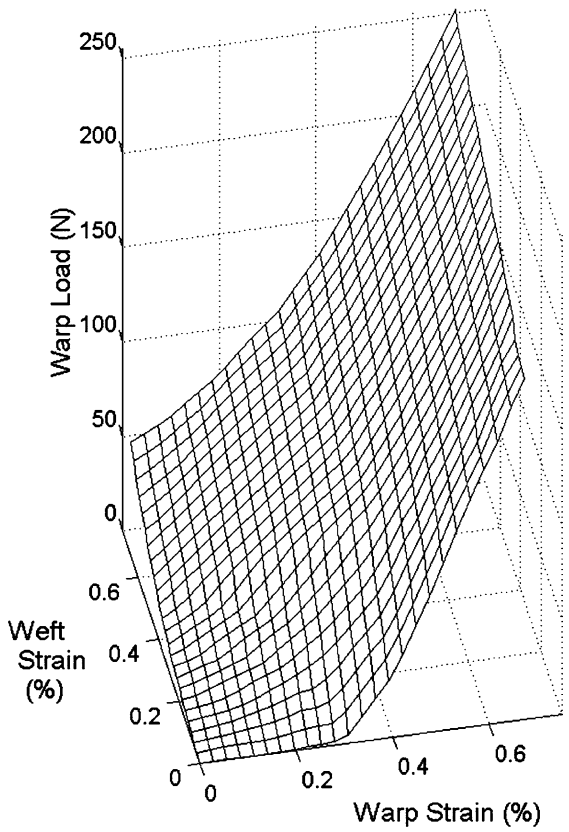

Fig. 3 Tension surface: Warp (or weft) tension in function of warp and weft axial strains

aspect of fabric biaxial tension (Fig. 5). It is because of this crushing that the tensile curve is non-linear in case of equi-biaxial tension ($k = 1$) (Fig. 6). Analyses of different woven unit cells (balanced and unbalanced) can be found in [25, 26] and in case of knitted materials in [38, 39]

Mesoscopic F.E. analysis of a woven unit cell under plane shearing

At macro scale, the fabric considered as a continuum is submitted to a pure in plane shear. Nevertheless, it can be

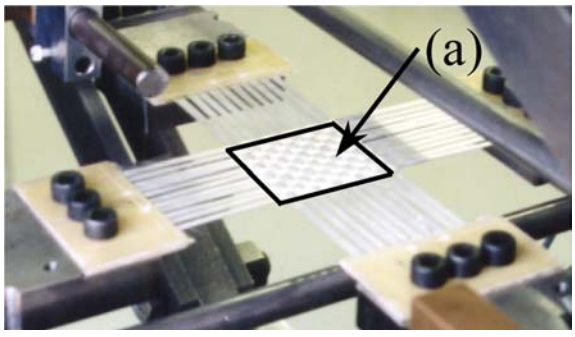

Fig. 4 Cross shape fabric specimen under biaxial tension test. (**a**) Active woven part of the specimen

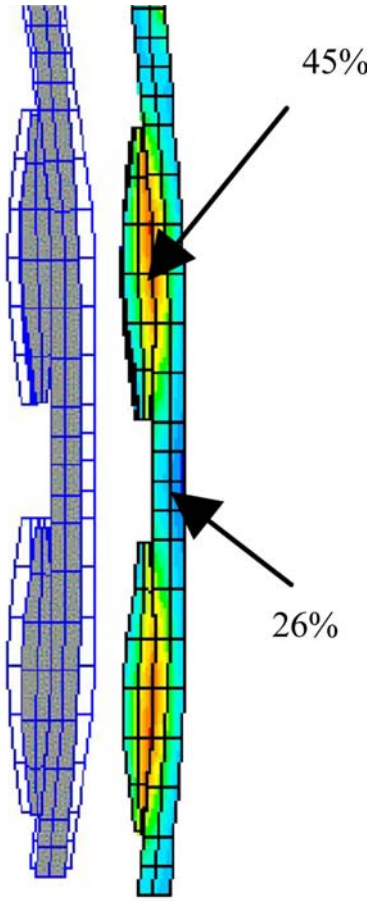

Fig. 5 Computed deformed shape and transverse logarithmic strain for an equi-biaxial load

shown by optical measurements on a single yarn (i.e. at mesoscale) that the yarns are not sheared but that they only rotate without internal strain before the shear angle locking angle is reached (Fig. 7a) [23]. When this locking angle is reached, the yarns are strained and especially laterally compressed (Fig. 7b). The kinematics of the picture frame are prescribed as boundary conditions on an elementary

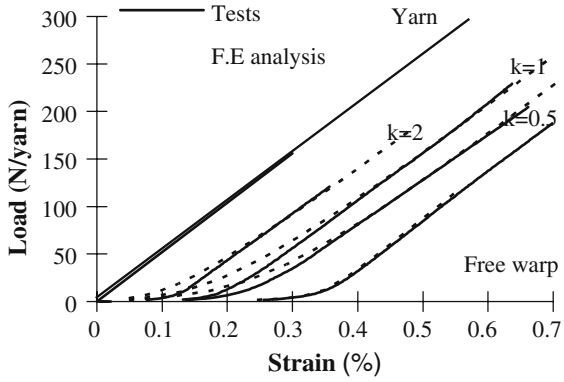

Fig. 6 Comparison between 3D finite element analyses of the woven cell under biaxial tension and biaxial tension experimental tests on cross shape specimens

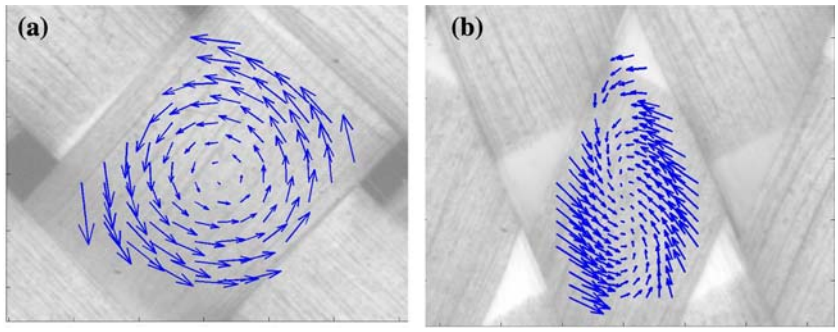

Fig. 7 Displacement field within the yarn obtained by optical measures. (**a**) Before the shear locking angle. (**b**) Beyond the shear locking angle

cell, but the yarn sections must stay perpendicular to the middle line before the locking angle. The result of an implicit finite element analysis is presented in Fig. 8 for a glass plain weave. It is compared with the experimental result obtained by a picture frame test [23, 40, 41]. The shear curve obtained by the F.E analysis is close to the experimental curve, but the analysis is stopped beyond 45° because of a lack of convergence. This is due to a problem of contact management. An explicit approach should probably allow to obtain the shear behaviour beyond the locking angle.

Simulation of woven reinforcement forming

Using the fabric behaviour in biaxial tension $T^{11}(\varepsilon_{11}, \varepsilon_{22})$, or $T^{22}(\varepsilon_{11}, \varepsilon_{22})$ determined as indicated in Section ''Mesoscopic F.E. analysis of woven unit cell under biaxial tension'' and the in plane shear behaviour C(γ) as indicated in Section ''Mesoscopic F.E. analysis of woven unit cell plane shearing'' in the element formulation presented Section ''Finite element made of woven cells'', fabric forming computations can be performed. The deep drawing of a square box is analysed. This test is a standard benchmark for sheet metal forming (the geometry of the tools is shown Fig. 9). It has been proposed at Numisheet 93 conference [42]. Accounting for the strongly non-developable geometry, this test is very severe especially for fabric forming because it asks very large angle variations between warp and weft yarns in the radiuses of the square box. If those radiuses are reduced, the shear strains that are necessary to shape the part become larger than the limit angle of the fabric. The forming of a fabric is simulated with the approach described above. Figure 10 presents the rotation angles between warp and weft directions and the deformed shape. Because the simulation concerns a forming process for which it is necessary to exceed the shear limit angle some wrinkle appear. The reason for these wrinkles is that they decrease the shear angle and consequently the strain energy. This simulation permits to know the minimum radius value necessary to avoid wrinkles for a given bank holder pressure. It also gives the values of angles between warp and weft yarns after forming. These angles are necessary for resin injection analyses and also for structural analyses of the composite part in service.

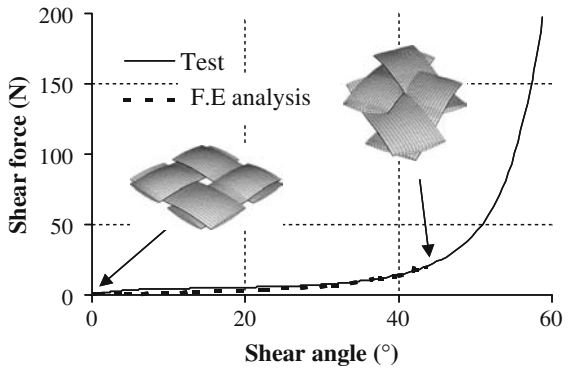

Fig. 8 Comparison between 3D finite element analyses of the woven cell under in plane shear and picture frame experimental tests

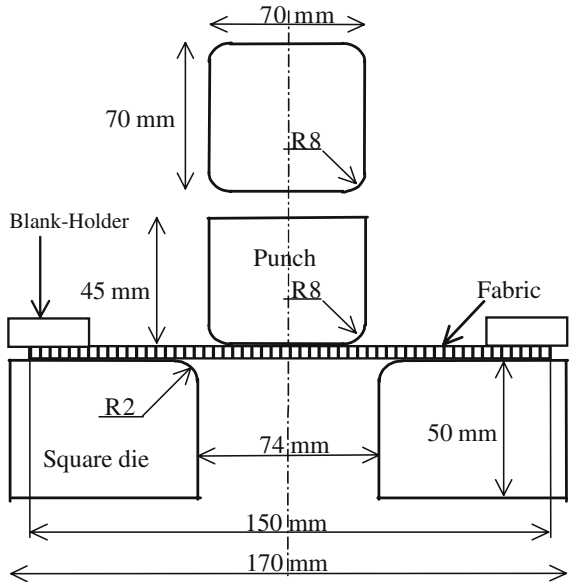

Fig. 9 Square box deep drawing. Geometry of the tools

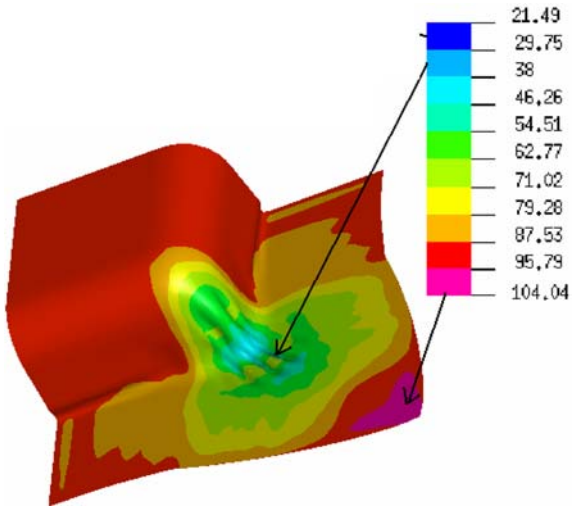

Fig. 10 Square box deep drawing. Deformed shape of the fabric and angles between warp and weft directions

Conclusions

A meso-macroscopic approach has been proposed for the simulation of woven composite reinforcement forming. The objective is to only compute the relevant quantities in the finite element made of woven cell. The interior nodal loads of the finite element are obtained from the strain field and from the in-plane biaxiale tensile behaviour and the in-plane shear behaviour. Those behaviours are computed by mesoscopic 3D analyses of the woven cell submitted respectively to tension and shear. These computations have proved to be consistent with experimental tests. The F.E. computations of the unit cell under shearing needs to be improved to give the shear curve beyond the shear locking angle. Some works are in progress at LaMCoS in order to achieve this goal by an explicit F.E. approach. The forming simulations made using the presented woven finite element permit to know the warp and weft angle after shaping and to describe possible wrinkles. The tensile energy mainly directs the forming before the shear locking angle is reached. Beyond this angle, the in plane shear stiffness is larger and leads to find geometrical solutions out of plane (i.e. wrinkles) in order to minimize the in-plane shear energy.

Acknowledgements The author acknowledge the support provided by the EADS aeronautical company and the researchers of his former laboratory: the LMSP Paris-Orléans.

References

1. Bickerton S, Simacek P, Guglielmi SE, Advani SG (1997) Comp Part A 28:801
2. Parnas RS (2000) Liquid composite molding. Hanser Garner publications
3. Van Der Ween F (1991) Intl J Numer Method Eng 31:1414
4. Long AC, Rudd CD (1994) I Mech E J Eng Manuf 208:269
5. Borouchaki H, Cherouat A (2002) Revue des composites et matériaux avancés, 12/3:407
6. Boisse P, Daniel JL, Hivet G, Soulat D (2001) Intl J Form Proc 3(3-4):351
7. Boisse Ph, Cherouat A, Gelin JC, Sabhi H (1995) Polymer Comp 16(1):83
8. De Luca P, Lefebure P, Pickett AK (1998) Comp Part A 29:101
9. Hsiao S-W, Kikuchi N (1999) Comp Met Appl Mech Eng 177:1
10. King MJ, Socrate S, Jearanaisilawong P (2005) Intl J Solids Struct 42:3867
11. Durville D (2002) Finite Element Euro Revue 11(2-3-4):463
12. Kawabata S, Niwa M, Kawai H (1973) J Textile Inst 64:21
13. Hivet G (2002) Modélisation mesoscopique du comportement biaxial et de la mise en forme des renforts de composites tissés, Ph.D. Thesis, University of Orléans
14. Lomov SV, Truong Chi T, Verpoest I, Peeters T, Roose D, Boisse P, Gasser A (2003) Intl J Form Proc 6(3-4):413
15. Sagar TV, Potluri P, Hearle JWS (2003) Comp Mater Sci 28:49
16. Ben Boubaker B, Haussy B, Ganghoffer JF (2002) CRAS Paris Mech Ser 330:871
17. Ben Boubaker B, Haussy B, Ganghoffer JF (2005) Euro J Comp Mech 14(6–7):653
18. Spencer AJM (2000) Comp Part A 31:1311
19. Xue P, Peng X, Cao J (2003) Comp Part A 34:183
20. Yu X, Ye L, Mai Y-W (2004) Proceedings of the Int. Conf ESAFORM 7, Trondheim, pp 325–328
21. Zouari B, Daniel JL, Boisse P (2005) Comp Struct 84:351
22. Buet-Gautier K, Boisse P (2001) Exp Mech 41:260
23. Dumont F (2003) Contribution à l'expérimentation et à la modélisation du comportement mécanique de renforts de composites tissés', Ph.D. Thesis, Université Paris 6
24. Lomov SV, Stoilova T, Verpoest I (2004) In: Proceedings of the Int. Conf ESAFORM 7, Trondheim
25. Gasser A, Boisse P, Hanklar S (2000) Comput Mater Sci 17:7
26. Boisse P, Gasser A, Hivet G (2001) Comp Part A 32:1395
27. Schnur DS, Zabaras N (1992) Intl J Numer Met Eng 33:2039
28. Gutowski TG (1985) SAMPE Quart 16(4):58
29. Baoxing C, Chou TW (1999) Composite Sci Tech 59:1519
30. Hughes TJR (1987) The finite element method, Linear Static and Dynamic finite element Analysis. Prentice Hall
31. Flanagan DP, Belytschko T (1981) Intl J Numer Met Eng 17:679
32. Pian TH, Chen DO (1983) Intl J Numer Met Eng 19:1741
33. Gilormini P, Roudier P, Abaqus and finite strain (1993) Internal report, LMT Cachan 140
34. Dafalias YF (1983) Trans ASME J Ap Mech 50:561
35. Gilormini P, Roudier P, Rougee P (1993) Comptes-rendus à l' Académie des Sciences de Paris 316(II):1659
36. Dienes JK (1979) Acta Mech 32:217
37. Crisfield MA (1991) Non linear finite element analysis of solids and structures, vol. II: Advanced topics. John Wiley & Sons, England
38. Hagege B (2004) Simulation du comportement mecanique des renforts fibreux en grandes transformations : application aux renforts tricotes, Ph.D. Thesis, ENSAM Paris
39. Hagège B, Boisse P, Billoët J-L (2005) Euro J Comp Mech 14(6–7):767
40. Mcbride TM, Chen J (1997) Comp Sci Technol 57:345
41. Mcguinness GB, O'Bradaigh CMO (1998) Comp Part A 29 (1–2):115
42. Numisheet '93 (1993) In: Makinouchi A, Nakamachi E, Onate E, Wagoner, RH (eds) Numerical simulation of 3-D sheet metal forming processes—Verification of simulation with experiments, Japan